Available online at www.sciencedirect.com
SCIENCE DIRECT
ELSEVIER
Journal of Inorganic Biochemistry xxx (2005) xxx–xxx
JOURNAL OF Inorganic Biochemistry
www.elsevier.com/locate/jinorgbio

Sulfur K-edge extended X-ray absorption fine structure spectroscopy of homoleptic thiolato complexes with Zn(II) and Cd(II)

Yuki Matsunaga [a], Kiyoshi Fujisawa [a,*], Naoko Ibi [a], Mitsuharu Fujita [a], Tetuya Ohashi [a] Nagina Amir [a], Yoshitaro Miyashita [a], Ken-ichi Aika [b], Yasuo Izumi [b,*], Ken-ichi Okamoto [a]

[a] *Graduate School of Pure and Applied Sciences, Department of Chemistry, University of Tsukuba, Tsukuba 305-8571, Japan*
[b] *Interdisciplinary Graduate School of Science and Engineering, Tokyo Institute of Technology, Yokohama 226-8502, Japan*

Received 6 February 2005; received in revised form 6 November 2005; accepted 9 November 2005

Abstract

The sulfur K-edge extended X-ray absorption fine structure (EXAFS) spectroscopy is applied to homoleptic thiolato complexes with Zn(II) and Cd(II), $(Et_4N)[Zn(SAd)_3]$ (**1**), $(Et_4N)_2[\{Zn(ScHex)_2\}_2(\mu\text{-}ScHex)_2]$ (**2**), $(Et_4N)_2[\{Cd(ScHex)_2\}_2(\mu\text{-}ScHex)_2]$ (**3**), $(Et_4N)_2[\{Cd(ScHex)\}_4(\mu\text{-}ScHex)_6]$ (**4**), $[Zn(\mu\text{-}SAd)_2]_n$ (**5**), and $[Cd(\mu\text{-}SAd)_2]_n$ (**6**) (HSAd = 1-adamantanethiol, HScHex = cyclohexanethiol). The EXAFS results are consistent with the X-ray crystal data of **1**–**4**. The structures of **5** and **6**, which have not been determined by X-ray crystallography, are proposed to be polynuclear structures on the basis of the sulfur K-edge EXAFS, far-IR spectra, and elemental analysis. Clear evidences of the S···S interactions (between bridging atoms or neighboring sulfur atoms) and the S···C_{far} interactions (in which C_{far} atom is next to carbon atom directly bonded to sulfur atom) were observed in the EXAFS data for all complexes and thus lead to the reliable determination of the structures of **5** and **6** in combination with conventional zinc K-edge EXAFS analysis for **5**. This new methodology, sulfur K-edge EXAFS, could be applied for the structural determination of in vivo metalloproteins as well as inorganic compounds.

Keywords: Extended X-ray absorption fine structure spectroscopy; Zinc(II); Cadmium(II); Molecular structure; M–S stretching

1. Introduction

Group 12 metal(II) complexes have not been paid much attention in the fundamental studies on vibrational energies as well as charge transfer (CT) transition energies. These metals consist of closed d^{10} electronic configuration and their ligands usually contain aromatic ring(s) or multiple bond(s) for the stabilization of Zn(II) and Cd(II) complexes. Therefore, it is difficult to uniquely assign vibration energies and CT transition energies for the series of complexes. The crystal structures of many thiolato complexes with Zn(II) and Cd(II) ions have been published [1–3]. In contrast, so far there have been only a few reports on systematic studies on the properties of group 12 metal(II) ions, using multinuclear nuclear magnetic resonance (NMR) spectroscopy such as ^{67}Zn NMR [4,5], ^{113}Cd NMR [6], and ^{199}Hg NMR [7] and resonance Raman spectroscopy [8]. In this situation, our strategy is to synthesize group 12 metal(II) complexes with "saturated" supporting ligands which do not contain double/triple bond(s) and have lower molecular weight. By using saturated supporting ligands, we recently reported the crystal structures together with vibrational energies and CT energies [9,10]. For Zn(II) complexes with S-containing saturated ligands such as 1-adamantanethiol (HSAd) and cyclohexanethiol (HScHex), the assignments of $(Et_4N)[Zn(SAd)_3]$ (**1**) and $(Et_4N)_2[\{Zn(ScHex)_2\}_2(\mu\text{-}ScHex)_2]$ (**2**) were very easy for the vibration energies by far-IR and Raman spectroscopies and for the CT energies by UV–visible (UV–Vis) absorp-

* Corresponding authors. Tel.: +81 29 853 6922; fax: +81 29 853 6503 (K. Fujisawa), +81 45 924 5569 (Y. Izumi).
E-mail addresses: kiyoshif@chem.tsukuba.ac.jp (K. Fujisawa), yizumi@chemenv.titech.ac.jp (Y. Izumi).

0162-0134/$ - see front matter © 2005 Elsevier Inc. All rights reserved.
doi:10.1016/j.jinorgbio.2005.11.004

tion spectroscopy [11]. The sulfur chemistry is related to various fields such as organic, inorganic chemistry, biochemistry, and environmental science. Therefore, these fundamental data of physicochemical properties for Zn(II) and Cd(II) complexes with saturated ligands should provide new insights into these research fields.

X-ray absorption spectroscopy (XAS) can characterize the coordination environment around a target atom. XAS has been applied to a variety of system such as inorganic compounds, catalysts, semiconductors, and biochemistry. Both metal K- and L-edges can be studied for the electronic transitions from metal 1s and from metal 2p, respectively. For example, the zinc K and $L_{I,II,III}$ absorption edges are at 9663 eV and at 1200, 1047, and 1024 eV, respectively. Other options of the X-ray absorption edges are the ligand K- and L-edges which excite the electron out of ligand 1s and 2p orbitals, respectively. The ligand K-edge XAS has been used to define the covalency of the ligand–metal bond in bioinorganic chemistry [12,13].

For the study of metal sites that have an unfilled d orbital, metal K/L-edge X-ray absorption near edge structure (XANES) are very effective. The pre-edge feature directly reflects unfilled d orbital(s) condition of each metal site. In contrast, as the Zn(II) and Cd(II) complexes contain d^{10} electronic configuration [14], metal K-edge XANES is not direct to determine the site symmetry and electronic state. On the other hand, extended X-ray absorption fine structure (EXAFS) provides detailed information about the bonding of ligand(s). Thus, zinc K-edge EXAFS has been applied to various fields, such as metalloproteins [14–18], semiconductor [19,20], medicine [21], and catalyst [22,23].

As the sulfur K-edge energy is relatively low (2471 eV) compared with that of metal, the photon flux from synchrotron radiation is relatively low, and thus the measurements take relatively longer accumulation time. However, this method can provide *direct* information about sulfur atom environment in proteins and metal complexes that cannot be obtained by the complementary metal K-edge measurements. The sulfur K-edge EXAFS has been applied already to inorganic materials [24–29] and metalloprotein [14,30]. However, no sulfur K-edge EXAFS studies of Zn(II) and Cd(II) complexes have been reported yet to our knowledge, in contrast, various Zn(II) and Cd(II) complexes mimicking biological systems do exist.

In our lower molecular weight complexes with saturated supporting ligands, the sulfur atoms occupy relatively higher weight ratio and the sulfur K-edge EXAFS measurements are easy. We discuss in this paper the sulfur K-edge EXAFS data of Zn(II) and Cd(II) complexes with saturated ligands such as **1**, **2**, $(Et_4N)_2[\{Cd(ScHex)_2\}_2(\mu\text{-}ScHex)_2]$ (**3**), and $(Et_4N)_2[\{Cd(ScHex)\}_4(\mu\text{-}ScHex)_6]$ (**4**) and the determination of their bond distances from sulfur atoms. The complementary zinc K-edge EXAFS of **1**, **2**, and **5** are also described. We propose the structures of $[Zn(\mu\text{-}SAd)_2]_n$ (**5**) and $[Cd(\mu\text{-}SAd)_2]_n$ (**6**) based on their sulfur K-edge and far-IR spectra, and elemental analysis. We also report the crystal structure of **4** and the M–S stretching vibration data for **3**–**6** in detail.

2. Results and discussion

2.1. General aspects

Complexes **1**–**3** were synthesized by the reported methods [11,31]. There are some differences in the reactivities between Zn(II) and Cd(II) complexes. The three-coordinate Cd(II) complex ($[Cd(SAd)_3]^-$) corresponding to **1** was not obtained. The complexes **2** and **3** have the same structures as reported, confirmed by UV–Vis, far-IR spectra, and elemental analysis. Tetranuclear Cd(II) complex **4** was obtained from the filtrate after filtration of **3**. The tetranuclear Zn(II) complex ($[\{Zn(ScHex)\}_4(\mu\text{-}ScHex)_6]^{2-}$) corresponding to **4** was not obtained. Complexes **5** and **6** were immediately formed as white powder after the addition of MCl_2 (M = Zn(II) and Cd(II)) solution to the NaSAd solution (MCl_2:NaSAd = 1:2). Complexes **5** and **6** were not dissolved in any solvents. Slow conversions from **1** to **5** and from **3** to **4** were observed in solution. Therefore, all complexes are studied in solid state in this paper (see Scheme 1).

2.2. Crystal structures

The crystal structures of **1**–**3** were reported and their simplified models are shown in Fig. 1 [11,31]. Complex **1** has a three-coordinate planar structure with three 1-adamantanethiolate anions and **2** has a dinuclear structure containing two ZnS_3 units bridged by two sulfur atoms from cyclohexanethiolate anions. In **1**, three sulfur atoms and one Zn(II) ion exist in the same plane (av. Zn–S: 2.262(4), av. S···S: 3.917(4), av. S–C: 1.844(9), av. S···C_{far}: 2.770(9) Å) [11]. In this paper, C_{far} is defined as the carbon atom next to the carbon atom which directly bonded to sulfur atom. The S–Zn–S angles in **1** are almost 120°, indicating a trigonal plane. In **2**, the Zn_2S_6 core has a D_{2h} symmetry (av. Zn–S: 2.352(1), av. S···S: 3.864(2), av. S–C: 1.831(5), av. S···C_{far}: 2.779(5) Å) [11]. The Cd(II) complex **3** has a dinuclear structure as same as **2** (av. Cd–S: 2.550(4), av. S···S: 4.136(6), av. S–C: 1.848(17), av. S···C_{far}: 2.75(1) Å) [31].

The crystal structure of **4** is shown in Fig. 2. Selected distances and angles of **4** are summarized in Table 1. Four Cd(II) ions and six sulfur atoms from cyclohexanethiolate

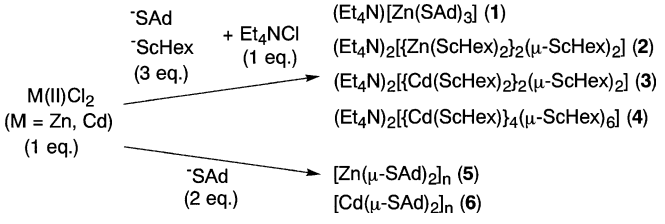

Scheme 1.

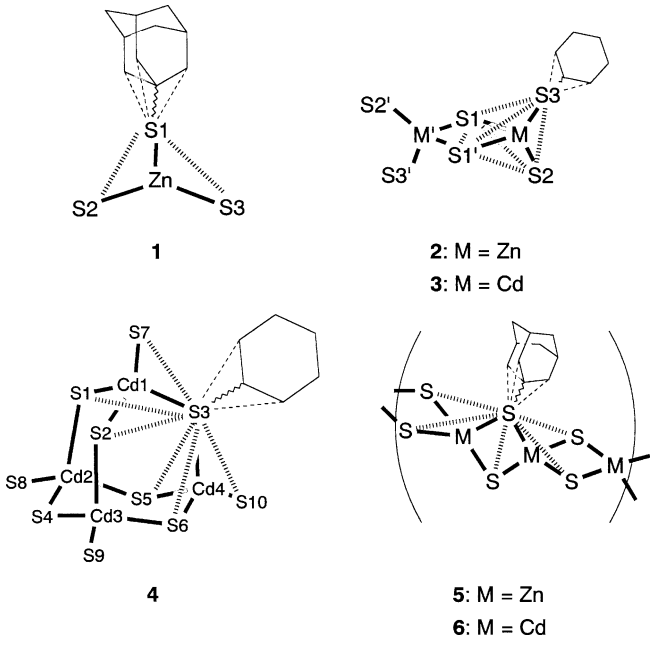

Fig. 1. Simplified structures of **1**–**6**. ((▬) for M–S, (∿∿) for S–C, (▪▪▪▪▪) for S···S, and (------) for S···C_{far}).

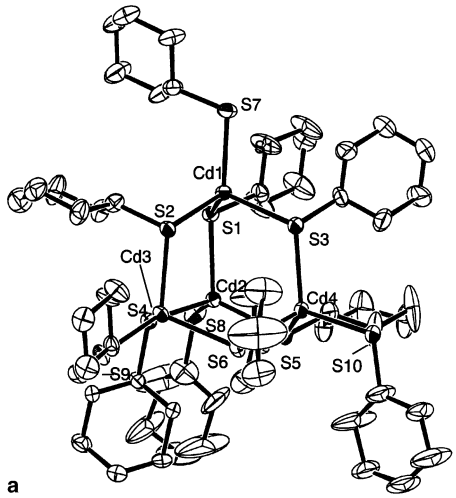

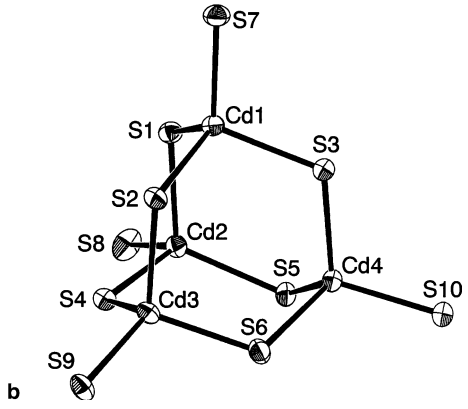

Fig. 2. ORTEP diagram of the anion of $(Et_4N)_2[\{Cd(ScHex)\}_4(\mu\text{-}ScHex)_6]$ (**4**). Non-H atoms are represented with 50% probability ellipsoids: (a) the whole structure and (b) the framework of Cd_4S_{10} unit.

ligand constitute a Cd_4S_6 adamantane-like cage. Each Cd(II) ion consists of a tetrahedral configuration, one terminal (the outside of adamantane-like cage) and three bridging cyclohexanethiolate ligands. The M_4X_{10} complexes containing adamantane-like cages have been reported for many metal ions and ligands. For example, the structures of $[(\mu\text{-}SPh)_6(MSPh)_4]^{2-}$ (M = Mn(II), Fe(II), and Co(II)) have been determined [32–36]. For Zn(II) and Cd(II) ions, the structures of $[(\mu\text{-}SPh)_6(MSPh)_4]^{2-}$ type complexes have been studied well as good structural models of metallothionein [37–39], including $[M_4(o\text{-}SC_6H_4CH_3)_{10}]^{2-}$ (M = Zn(II) and Cd(II)) [40], and $[Zn_4(SePh)_{10}]^{2-}$ [41]. $[(\mu\text{-}SR)_6(MX)_4]$ type complexes were reported from a structural viewpoint. The terminal positions on the adamantane-like cage can be substituted by other ligands such as sulfide $[S_4M_{10}(SPh)_{16}]^{2-}$ (M = Zn(II) and Cd(II)) [42,43], halogenide ions $[(\mu\text{-}SPh)_6(ZnX)_4]^{2-}$ (X = Cl, Br, and I) [44], $[(\mu\text{-}SPh)_6(ZnSPh)_2(ZnCl)_2]^{2-}$ [45], $[(\mu\text{-}S\text{-}i\text{Pr})_6(CdBr)_4]^{2-}$ [46], $[(\mu\text{-}EPh)_6(CdBr)_4]^{2-}$ (E = S and Se) [47], and phosphine $[(\mu\text{-}S\text{-}i\text{Pr})_6(CdPPh_3)_2(CdOClO_3)_2]$ [48]. The complex substituted by solvent, $[(\mu\text{-}SPh)_6Zn_4(SPh)(CH_3OH)]^-$ [49], was also structurally characterized.

Bond distances of Cd–S_t (2.485(2)–2.502(3) Å) and Cd–S_b (2.542(2)–2.576(3) Å) in **4** are in the same range as those of Cd–S_t (2.460(4)–2.480(3) Å) and Cd–S_b (2.533(3)–2.603(3) Å) in $[Cd_4(SPh)_{10}]^{2-}$ [39]. Bond distances of $S_b\cdots S_b$ (3.896(3)–4.355(3) Å) and $S_b\cdots S_t$ (4.052(4)–4.349(4) Å) in **4** are also in the same range as those of $S_b\cdots S_b$ (3.695(4)–4.434(4) Å) and $S_b\cdots S_t$ (3.96–4.36 Å) in $[Cd_4(SPh)_{10}]^{2-}$ [39]. On the other hand, bond angles of S_t–Cd–S_b (101.84(7)–118.38(8)°) and S_b–Cd–S_b (99.35(7)–115.83(8)°) in **4** were not common to $[Cd_4(SPh)_{10}]^{2-}$ (S_t–Cd–S_b (102.0(1)–121.1(1)°) and S_b–Cd–S_b (91.5(1)–118.4(1)°)) [39]. This is due to the differences of using ligands between alkyl and aromatic frameworks. From these differences, the corresponding cluster such as $[Zn_4(ScHex)_{10}]^{2-}$ could not be synthesized by any experimental conditions [37–39]. Each Cd(II) center is a distorted tetrahedral CdS_4. Three sulfur atoms (S4, S5, and S6) and three Cd(II) ions (Cd2, Cd3, and Cd4) constitute a chair-like $Cd_3(\mu\text{-}S)_3$ ring. This unit is related to metallothioneins; a mammalian Cd(II) substituted metallothionein contains a $Cd_3(Cys\text{-}S)_9$ and a $Cd_4(Cys\text{-}S)_{11}$ units, both including a $Cd_3(\mu\text{-}S)_3$ ring [1,37,39]. Comparing with **3**, the bond distances in **4** (av. Cd–S: 2.547(7), av. $S_b/S_t\cdots S_b/S_t$: 4.13(1), S–C: 1.827(19), S···C_{far}: 2.75(3) Å) are almost the same as those in **3** (av. Cd–S: 2.550(4), av. $S_t\cdots S$ 4.136(6), S–C: 1.848(17), S···C_{far}: 2.75(1) Å). This indicates that these bond distances do not affect on each structure.

2.3. Far-IR spectroscopy

The far-IR spectra of **4** along with **2** and **3**, which contain cyclohexanethiolate ligand, are shown in Fig. 3. There are many peaks arising from thiolate ligands below 360 cm^{-1} because of the presence of terminal and bridging

Table 1
Selected distances (Å) and angles (°) for $(Et_4N)_2[\{Cd(ScHex)\}_4(\mu\text{-}ScHex)_6]$ (**4**)

Distances					
Cd–S_t[a]					
Cd1–S7	2.495(2)	Cd3–S9	2.485(2)		
Cd2–S8	2.496(4)	Cd4–S10	2.502(3)	Mean	2.495(4)
Cd–S_b[a]					
Cd1–S1	2.576(3)	Cd2–S4	2.547(2)	Cd3–S6	2.559(3)
Cd1–S2	2.562(2)	Cd2–S5	2.575(3)	Cd4–S3	2.568(2)
Cd1–S3	2.575(3)	Cd3–S2	2.567(2)	Cd4–S5	2.572(3)
Cd2–S1	2.563(2)	Cd3–S4	2.567(3)	Cd4–S6	2.542(2)
				Mean	2.564(3)
Cd···Cd					
Cd1–Cd2	4.2077(9)	Cd1–Cd4	4.2698(9)	Cd2–Cd4	4.203(1)
Cd1–Cd3	4.2851(7)	Cd2–Cd3	4.3535(9)	Cd3–Cd4	4.3329(9)
				Mean	4.275(1)
S_b···S_b					
S1–S2	4.286(3)	S2–S3	3.934(3)	S3–S6	4.101(3)
S1–S3	4.275(4)	S2–S4	3.985(3)	S4–S5	4.218(3)
S1–S4	3.896(3)	S2–S6	4.123(3)	S4–S6	4.076(4)
S1–S5	4.327(3)	S3–S5	4.355(3)	S5–S6	3.928(4)
				Mean	4.125(4)
S_b···S_t					
S1–S7	4.217(3)	S4–S8	4.149(4)	S6–S9	4.193(3)
S2–S7	4.169(3)	S5–S8	4.275(5)	S3–S10	4.052(4)
S3–S7	4.083(4)	S2–S9	4.338(3)	S5–S10	4.349(4)
S1–S8	4.018(4)	S4–S9	4.152(3)	S6–S10	4.109(3)
				Mean	4.175(5)
S–C					
S1–C11	1.842(9)	S5–C51	1.85(1)	S8–C81	1.77(1)
S2–C21	1.86(1)	S6–C61	1.84(2)	S9–C91	1.80(1)
S3–C31	1.839(9)	S7–C71	1.85(1)	S10–C101	1.79(2)
S4–C41	1.825(8)			Mean	1.83(2)
Angles					
S_t–Cd–S_b					
S1–Cd1–S7	112.50(8)	S4–Cd2–S8	110.70(9)	S2–Cd3–S6	107.10(8)
S2–Cd1–S7	111.05(8)	S5–Cd2–S8	114.87(9)	S3–Cd4–S10	106.09(8)
S3–Cd1–S7	107.27(8)	S2–Cd3–S9	118.38(8)	S5–Cd4–S10	117.95(9)
S1–Cd2–S8	105.16(9)	S2–Cd3–S4	101.84(7)	S6–Cd4–S10	109.11(8)
				Mean	110.17(9)
S_b–Cd–S_b					
S1–Cd1–S2	113.06(7)	S1–Cd2–S5	114.75(7)	S4–Cd3–S6	105.32(8)
S1–Cd1–S3	112.21(8)	S4–Cd2–S5	110.84(8)	S3–Cd4–S5	115.83(8)
S2–Cd1–S3	99.96(8)	S2–Cd3–S4	101.84(7)	S3–Cd4–S6	106.76(8)
S1–Cd2–S4	99.35(7)	S2–Cd3–S6	107.10(8)	S5–Cd4–S6	100.35(8)
				Mean	107.28(8)
Cd–S_b–Cd					
Cd1–S1–Cd2	109.94(8)	Cd1–S3–Cd4	112.25(8)	Cd2–S5–Cd4	109.47(9)
Cd1–S2–Cd3	113.34(9)	Cd2–S4–Cd3	116.69(9)	Cd3–S6–Cd4	116.3(1)
				Mean	113.0(1)

[a] t, terminal ligand; b, bridging ligand.

sulfur atoms. The stretching vibration ν(Cd–S_t) and ν(Cd–S_b) bands in the spectrum of **3** (Fig. 3 (b)) are assigned at 352 and 220 cm^{-1}, respectively [11]. The spectra of **2** (Fig. 3 (a)) and **3** were very similar and the two bands corresponding to ν(M–S) shifted to lower energy from **2** (357 and 235 cm^{-1}) to **3** (352 and 220 cm^{-1}).

The structural change from **3** to **4** (Fig. 3 (c)) is reflected in the spectra. As for $(Me_4N)_2[Cd_4(SPh)_{10}]$, the Cd_4S_{10} core has a T_d symmetry and it is expected to show metal–ligand stretching vibrations with A_1 (Raman active) and T_2 (IR and Raman active) symmetry due to the four terminal ligands, and A_1 (Raman active) + E (Raman active) + T_1 (Raman active) + $2T_2$ (IR and Raman active) symmetry due to the six bridging ligands [50]. In addition, the spectrum of **4** is broadened compared to that of **3** in the whole region. By comparing with the far-IR and Raman spectra,

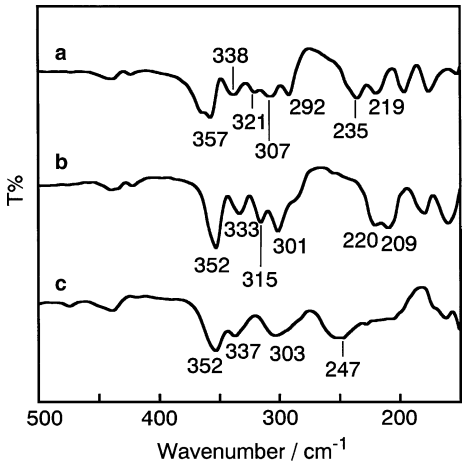

Fig. 3. Far-IR spectra: (a) $(Et_4N)_2[\{Zn(ScHex)_2\}_2(\mu\text{-}ScHex)_2]$ (**2**), (b) $(Et_4N)_2[\{Cd(ScHex)_2\}_2(\mu\text{-}ScHex)_2]$ (**3**), and (c) $(Et_4N)_2[\{Cd(ScHex)\}_4(\mu\text{-}ScHex)_6]$ (**4**).

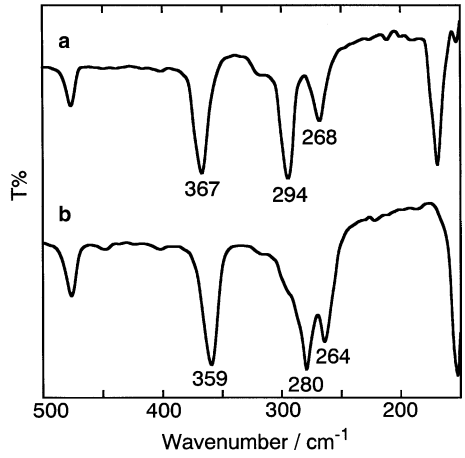

Fig. 4. Far-IR spectra: (a) $[Zn(\mu\text{-}SAd)_2]_n$ (**5**) and (b) $[Cd(\mu\text{-}SAd)_2]_n$ (**6**).

the bands at 352 and 303 cm^{-1} in **4** were assigned to ν(Cd–S_t), and the newly formed band at 247 cm^{-1} was assigned to ν(Cd–S_b).

The structures of **5** and **6** were studied by far-IR spectra. Each spectrum shows similar patterns as shown in Fig. 4. Three strong bands shifted toward lower energy side from Zn(II) complex **5** to Cd(II) complex **6**. Two of them at 367 and 294 cm^{-1} in the spectrum of **5**, which show larger shifts (difference 8–14 cm^{-1}) rather than the third one (difference 4 cm^{-1}), are assigned to ν(Zn–S). In the spectrum of **6**, the bands at 359 and 280 cm^{-1} are assigned to ν(Cd–S). Elemental analysis supported that **5** and **6** have the same composition containing an $[M(SAd)_2]$ framework.

2.4. Zinc K-edge EXAFS spectroscopy

The zinc K-edge EXAFS spectra were measured for **1**, **2**, and **5**. The k^3-weighted EXAFS oscillation data and its associated Fourier transforms in comparison with each fitting data are shown in Figs. S1–S3 (see Supporting Information). The obtained interatomic distances, Debye–Waller factors, and coordination numbers are summarized in Table S1 (see Supporting Information). For **1** and **2**, the EXAFS best fit data reproduced well the Zn–S bond distances and the interactions between Zn(II) ions and carbon atoms near sulfur atoms: Zn–S bond distances (2.259 Å for **1** and 2.345 Å for **2**) and Zn···C bond distances (3.567 Å for **1** and 3.677 Å for **2**) comparing with the values in crystal structures. In particular, the interaction between two Zn(II) ions was observed for **2** at 3.326 Å with the coordination number of one. This peak strongly suggests the dinuclear structure in **2**. The EXAFS data of **5** was fit well when a structure model of a polynuclear bridged by sulfur atoms of 1-adamantanethiolate ions was assumed. The peak at 3.298 Å should be Zn···Zn based on the fit (Fig. S3). The fitting of **5** without Zn···Zn interaction gave a worse F value (18.993%) and the fit did not reproduce the peak in the range from 2.5 to 3.0 Å (data not shown). Far-IR and elemental analysis further support that **5** contains common $[Zn(SAd)_2]$ framework. We also conclude that this relatively stronger Zn···Zn interaction is very useful assignment by zinc K-edge EXAFS data for determining the structure as reported [11].

2.5. Sulfur K-edge EXAFS spectroscopy

The sulfur K-edge EXAFS Fourier transforms of **1**–**6** are shown in Figs. 5–10 with corresponding spectral fits. The obtained interatomic distances, Debye–Waller factors, and coordination numbers are summarized in Table 2. The EXAFS results of **1**–**4** are in good agreement with the crystallographic data. It is worthy to notice that S···S interactions were observed clearly for all the spectra. For **1**, S···S interactions between neighboring sulfur atoms (S1···S2, S1···S3, and S2···S3 in Fig. 1) appeared at 3.914 Å in Fig. 5, in good agreement with the crystal data (av. 3.917(4) Å). S···S interactions in the spectra of **2** (3.827 Å, Fig. 6) includes not only between terminal sulfur atoms (S2···S3) but also between bridging and terminal sulfur atoms (S1···S2 and S1···S3) and between bridging sulfur atoms (S1···S1′), all in good agreement with crystallographic data (av. 3.864(2) Å). In the case of **3** (Fig. 7), the S···S interaction was observed at 4.149 Å, which is in good agreement with the crystallographic data (av. 4.136(6) Å) [31]. In the crystal structure of **4** (Fig. 2), S···S distances (including S_b···S_b and S_b···S_t) range widely from 3.896(3) Å (S1···S4) to 4.355(3) Å (S3···S5). The EXAFS data fitting of **4** improves when the S···S interactions are divided into two parts as the shorter S···S interactions (3.896(3)–4.109(3) Å) and the longer one (4.123(3)–4.355(3) Å). The shorter and longer S···S interactions are fit at 3.992 and 4.263 Å, respectively (Fig. 8), consistent with the average distance of crystallographic data (av. 4.018(4) and av. 4.245(5) Å).

The S···S interaction of **1** was found to be longer than that of **2** (3.914 Å for **1**, 3.827 Å for **2**). This trend is due to the structural difference: **1**; planar and **2**; tetrahedral. The S···S interactions of **2** include two types: the shorter

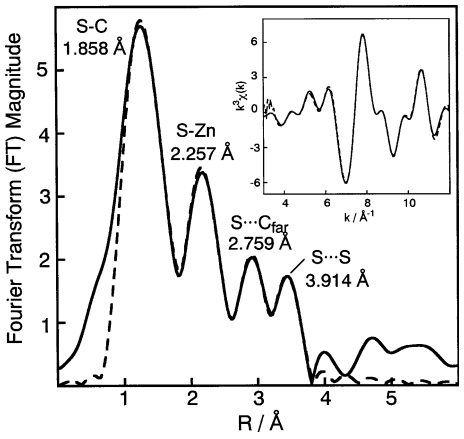

Fig. 5. Sulfur K-edge EXAFS Fourier transform of **1**; experimental (solid line) and the fit (dash line) data. (Inset: the k^3-weighted sulfur K-edge EXAFS of **1**; experimental (solid line) and the fit (dash line) data.)

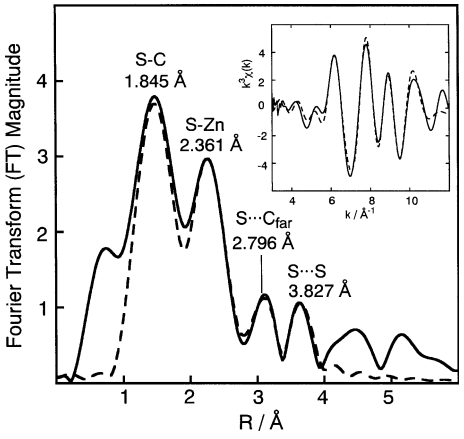

Fig. 6. Sulfur K-edge EXAFS Fourier transform of **2**; experimental (solid line) and the fit (dash line) data. (Inset: the k^3-weighted sulfur K-edge EXAFS of **2**; experimental (solid line) and the fit (dash line) data.)

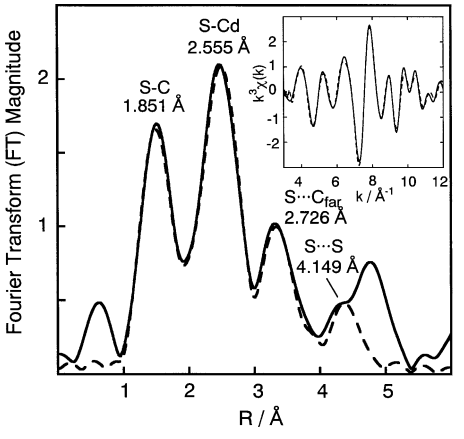

Fig. 7. Sulfur K-edge EXAFS Fourier transform of **3**; experimental (solid line) and the fit (dash line) data. (Inset: the k^3-weighted sulfur K-edge EXAFS of **3**; experimental (solid line) and the fit (dash line) data.)

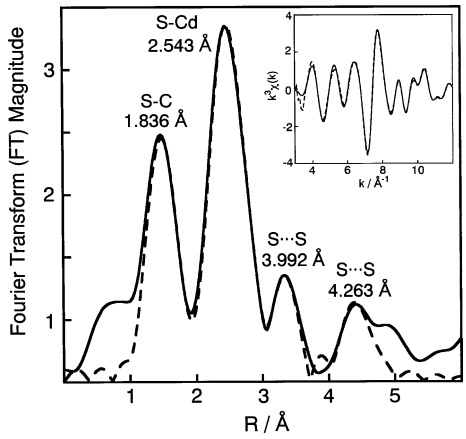

Fig. 8. Sulfur K-edge EXAFS Fourier transform of **4**; experimental (solid line) and the fit (dash line) data. (Inset: the k^3-weighted sulfur K-edge EXAFS of **4**; experimental (solid line) and the fit (dash line) data.)

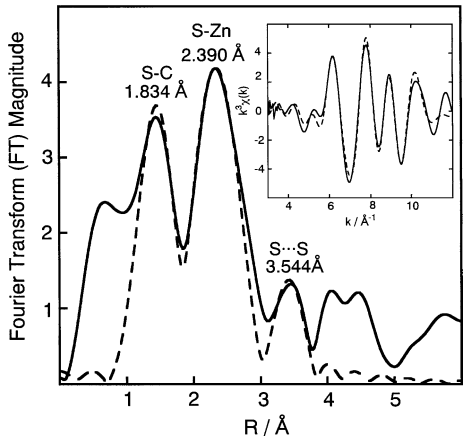

Fig. 9. Sulfur K-edge EXAFS Fourier transform of **5**; experimental (solid line) and the fit (dash line) data. (Inset: the k^3-weighted sulfur K-edge EXAFS of **5**; experimental (solid line) and the fit (dash line) data.)

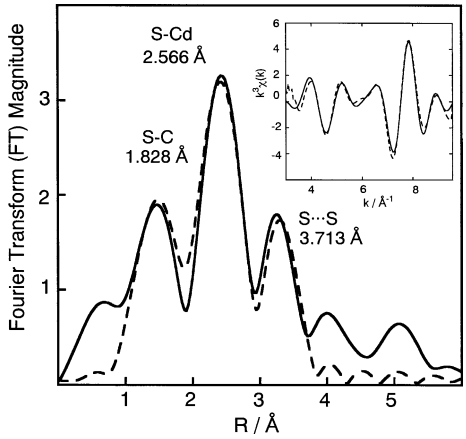

Fig. 10. Sulfur K-edge EXAFS Fourier transform of **6**; experimental (solid line) and the fit (dash line) data. (Inset: the k^3-weighted sulfur K-edge EXAFS of **6**; experimental (solid line) and the fit (dash line) data.)

distance of $S_b\cdots S_b$ at 3.594(2) Å and the longer distances of $S_b\cdots S_t$ and $S_t\cdots S_t$ ranging from 3.849(7) to 4.088(2) Å [11]. For the analogous complexes $[\{Zn(SR)_2\}_2(\mu\text{-}SR)_2]^{2-}$ (SR = SPh and SEt), the average S···S interaction is 3.835(9) Å for SR = SPh and 3.848(8) Å for SR = SEt [51,52]. Similarly to **2**, $S_b\cdots S_b$ distance was at 3.891(1) Å

Table 2
Coordination number (CN), interatomic distances (r, Å), Debye–Waller factors (σ^2, Å^2) and goodness of fit parameter (F, %) obtained from the best fits to the sulfur K-edge EXAFS data for **1**–**6**

Complex	Pair atom	CN	r (Å)	σ^2 (Å^2)	F[a] (%)	Average bond distance[b] (Å)	Reference
$(Et_4N)[Zn(SAd)_3]$ (**1**)	Zn	1	2.257	0.0034	1.106	2.262(4)	[11]
	S	2	3.914	0.0038		3.917(4)	
	C	1	1.858	0.0035		1.844(9)	
	C_{far}	3	2.759	0.0031		2.770(9)	
$(Et_4N)_2[\{Zn(ScHex)_2\}_2(\mu\text{-}ScHex)_2]$ (**2**)	Zn	1.33	2.361	0.0035	1.741	2.352(1)	[11]
	S	3.67	3.827	0.0026		3.864(2)	
	C	1	1.845	0.0038		1.831(5)	
	C_{far}	1	2.796	0.0021		2.779(5)	
$(Et_4N)_2[\{Cd(ScHex)_2\}_2(\mu\text{-}ScHex)_2]$ (**3**)	Cd	1.33	2.555	0.0035	2.255	2.550(4)	[31]
	S	3.67	4.149	0.0009		4.136(6)	
	C	1	1.851	0.0036		1.848(17)	
	C_{far}	2	2.726	0.0038		2.75(1)	
$(Et_4N)_2[\{Cd(ScHex)\}_4(\mu\text{-}ScHex)_6]$ (**4**)	Cd	1.67	2.543	0.0036	2.056	2.547(7)	This work
	S	4.8	3.992	0.0037		4.018(4)	
	S	4.8	4.263	0.0030		4.245(5)	
	C	1	1.836	0.0038		1.827(10)	
	C_{far}	2	2.761	0.0506		2.75(3)	
$[Zn(\mu\text{-}SAd)_2]_n$ (**5**)	Zn	2	2.390	0.0017	6.242		This work
	S	5	3.544	0.0034			
	C	1	1.834	0.0045			
	C_{far}	3	2.876	0.0213			
$[Cd(\mu\text{-}SAd)_2]_n$ (**6**)	Cd	2	2.566	0.0009	6.786		This work
	S	5	3.713	0.0146			
	C	1	1.828	0.0005			
	C_{far}	3	2.895	0.0306			

[a] $F = \{\sum(k^3\chi_{obs} - k^3\chi_{calc})^2/\sum(k^3\chi_{obs})^2\}^{1/2}$.
[b] Bond distances in crystallographic data.

and longer $S_b\cdots S_t$ and $S_t\cdots S_t$ ranging from 3.9507(6) to 4.3955(6) Å in the crystal structure of **3**. The average $S\cdots S$ interaction of $[\{Cd(SPh)_2\}_2(\mu\text{-}SPh)_2]^{2-}$ is 4.130(9) Å [51]. The $S\cdots S$ interactions of **4**, having a Cd_4S_6 adamantane-like cage, span a wide range 3.992 and 4.263 Å. Thus, the presence of $M_2(\mu\text{-}SR)_2$ core is predicted when the $S\cdots S$ interaction was at 3.8 and 4.1 Å for unknown Zn(II) and Cd(II) complexes, respectively. This $S\cdots S$ interaction by sulfur K-edge EXAFS could determine the equivalent structural information instead of measuring $Zn\cdots Zn$ interaction by zinc K-edge EXAFS. In addition, $S\cdots C_{far}$ interaction in Fig. 5 for **1** (2.759 Å), in Fig. 6 for **2** (2.796 Å) and Fig. 7 for **3** (2.726 Å), also contributes to settle these results by sulfur K-edge EXAFS.

The structures of **5** and **6** were determined based on the $S\cdots S$ and $S\cdots C_{far}$ distance values by the sulfur K-edge EXAFS fits. The structure of **5** and **6** includes the $[M(SAd)_2]$ framework from far-IR and elemental analysis as described above. In the XAS spectrum of **6**, an edge was observed at ~2850 eV, which should originate from trace amounts of chloride ions used in the synthesis. Thus, the spectrum limited in the 2520–2820 eV region was used throughout the fits for **6**. The fittings of **5** and **6** agreed fairly well with experimental data with small F values (6.242% for **5** and 6.786% for **6**) as shown in Fig. 9 for **5** and Fig. 10 for **6**. Moreover, for both complexes, the presence of $S\cdots S$ was convincing. The obtained $S\cdots S$ interaction distances of **5** and **6** (3.544 Å for **5** and 3.713 Å for **6**, respectively) are shorter than those of **2** (3.827 Å), **3** (4.149 Å), $[\{M(SPh)_2\}_2(\mu\text{-}SPh)_2]^{2-}$ (M = Zn(II) (3.835(9) Å) and Cd(II) (4.130(9) Å)), and $[\{Zn(SEt)_2\}_2(\mu\text{-}SEt)_2]^{2-}$ (3.848(8) Å) [52]. These results suggest that structures of **5** and **6** contain only $S_b\cdots S_b$ interaction similar to $S_b\cdots S_b$ of **2** (4.594(2) Å [11]) and **3** (3.891(1) Å [31]), and are much shorter than the $S_b\cdots S_t$ and $S_t\cdots S_t$. Thus, **5** and **6** are found to polynuclear structures. The S–M distance and $S\cdots S$ interaction of **6** (Cd(II) complex) are longer than those of **5** (Zn(II) complex). When the fitting was carried out without $S\cdots S$ interaction, F values are higher, 9.739% for **5**, 19.616% for **6** (data not shown). These data rule out the possibility of **5** and **6** being a mononuclear. The S–C and $S\cdots C_{far}$ distances are almost the same. Therefore, it is confirmed that these EXAFS curve fit data can be applied to clarify unknown structure.

For the fit of zinc K-edge EXAFS of **5**, three waves fit was performed. Complementarily, four waves nicely fit in the sulfur K-edge EXAFS for the same complex. The Zn–S bond was monitored by both from zinc 1s absorption (2.40 Å, Table S1) and from S 1s absorption (2.39 Å, Table 2). The distance values obtained were essentially identical. Thus in general, the sulfur K-edge EXAFS analyses in this paper are reliable.

3. Conclusion

The complexes with saturated sulfur containing ligands, **1**–**4**, were studied using the sulfur K-edge EXAFS spectroscopy. Both S···S and S···C_{far} interactions were detected clearly in the EXAFS analysis of **1**–**4**. We showed that this information could be used reliably for determining the structures either mononuclear or polynuclear. The structures of **5** and **6** can be determined by fitting the sulfur K-edge EXAFS, coupled with far-IR spectra and elemental analysis. The S···S interaction was observed in both EXAFS spectra which further supports that **5** and **6** have a polynuclear structure. It also indicates that the applied parameters should relate to each expected structure. To confirm the feasibility of sulfur K-edge EXAFS to homoleptic thiolato complexes having closed d^{10} electronic configuration, obtained data was compared to the results of zinc K-edge EXAFS spectroscopy as well-established method. The two methodologies were found to give complementary, consistent bonding information. In summary, the information obtained from the sulfur K-edge EXAFS spectroscopy would be useful for determining structures of various Zn(II) and Cd(II) complexes in combination with other spectroscopic data.

4. Experimental

$ZnCl_2$ and $CdCl_2 \cdot 2.5H_2O$ were obtained from Wako Pure Chemical Int. Ltd. $CDCl_3$ was purchased from Cambridge Isotope Laboratories Inc. All chemical reagents were used without further purification. Preparation and handling of all the complexes were performed under an argon atmosphere by employing standard Schlenk line techniques. Ethanol and methanol were commercially spectroscopic grade and used after bubbling argon gas. Acetonitrile and dichloromethane were distilled from CaH_2 and P_2O_5 prior to use, respectively. Diethyl ether was carefully purified by refluxing/distilling under an argon atmosphere over sodium benzophenone ketyl [53].

IR or far-IR spectra were recorded on KBr pellets in the region of 4600–400 cm^{-1} or CsI pellets in the region of 650–100 cm^{-1} using a JASCO FT/IR-550 spectrophotometer, respectively. FT-Raman spectra were measured using KBr or neat pellets on a Perkin–Elmer Spectrum GX spectrophotometer. Abbreviations used in the description of vibration data are as follows: vs, very strong; s, strong; m, medium, w, weak. UV–Vis spectra of solution state were recorded with a JASCO V-570 spectrophotometer at room temperature using a quartz cell (1 mm path length) in the region of 200–500 nm. UV–Vis spectra of solid state were recorded using the fine powder mull samples, which were prepared by finely grinding the solid materials, with a JASCO V-560 spectrophotometer in the region of 200–500 nm. These were suspended in mineral oil (poly(dimethylsiloxane), Aldrich) and spread between quartz plates. Elemental analysis (C, H, N) was performed by the Chemical Analysis Center of the University of Tsukuba.

4.1. Synthesis

Complexes **1** and **2** were synthesized by the method reported earlier [11]. 1-Adamantanethiol (HSAd) was synthesized by the same procedure following Refs. [54,55]. NaSAd and NaScHex were formed by the reaction of HSAd and HScHex with 0.8 eq. of NaH in diethyl ether, respectively.

*$(Et_4N)_2[\{Cd(ScHex)_2\}_2(\mu\text{-}ScHex)_2]$ (**3**) and $(Et_4N)_2[\{Cd(ScHex)\}_4(\mu\text{-}ScHex)_6]$ (**4**).* The synthesis of **3** was carried out by the reported method [31] by using of $CdCl_2 \cdot 2.5H_2O$ (0.228 g, 1.0 mmol), NaScHex (0.443 g, 3.20 mmol), and Et_4NCl (0.183 g, 1.10 mmol) in the mixed solvent of acetonitrile and ethanol. The colorless crystals of **3** were formed from diethyl ether and acetonitrile. The colorless crystals of **4** suitable for X-ray analysis were formed from the solution after **3** was removed at −30 °C (0.430 g, 21% yield). For **3**; Anal. Calcd. for $C_{52}H_{106}N_2Cd_2S_6$: C, 53.08; H, 9.08; N, 2.38%. Found: C, 52.81; H, 9.00; N, 2.51%. IR ν/cm^{-1} (KBr): 3423m, 2918vs, 1487m, 1443m, 1394m, 1171m, 997m, 784m. far-IR ν/cm^{-1} (CsI): 514w, 439w, 352vs, 333m, 315m, 301m, 220m, 209m, 181m. UV–Vis λ/nm (CH_3CN): 246. For **4**; Anal. Calcd. for $C_{72}H_{154}N_2Cd_4S_{10}O_2$ (**4** · $2H_2O$): C, 46.74; H, 8.39; N, 1.51%. Found: C, 46.87; H, 7.95; N, 1.39%. IR ν/cm^{-1} (KBr): 3435m, 2922vs, 2848s, 1482w, 1445m, 1260m, 1200m, 1172m, 997m, 817w, 729w. far-IR ν/cm^{-1} (CsI): 514m, 474w, 438w, 352vs, 337m, 303m, 247m, 227w. Raman shift ν/cm^{-1}: 515w, 438w, 364s, 357vs, 338m, 321m, 307m, 292m, 235m, 219m, 195m, 176m. UV–Vis λ/nm (CH_3CN): 212.

*$[Zn(\mu\text{-}SAd)_2]_n$ (**5**).* $ZnCl_2$ (0.307 g, 2.25 mmol) dissolved in methanol (15 mL) was added to the NaSAd (0.942 g, 4.95 mmol) solution in methanol (15 mL). The white powder was immediately formed. After stirring the mixture for several hours, the solution was concentrated to dryness. The residue was washed with dichloromethane, water and methanol (0.507 g, 56% yield). Anal. Calcd. for $C_{21}H_{34}S_2OZn$ (**5** · CH_3OH): C, 58.38; H, 7.93%. Found: C, 58.59; H, 7.56%. IR ν/cm^{-1} (KBr): 2903vs, 2847m, 1448w, 1297w, 1101w, 1037m, 830w, 684w. far-IR ν/cm^{-1} (CsI): 476m, 367vs, 294vs, 268m, 168s. Raman shift ν/cm^{-1}: 479m, 402m, 372s, 253vs. UV–Vis λ/nm (solid): 219.

*$[Cd(\mu\text{-}SAd)_2]_n$ (**6**).* $CdCl_2 \cdot 2.5H_2O$ (0.280 g, 1.23 mmol) dissolved in methanol (15 mL) was added to the NaSAd (0.499 g, 2.62 mmol) solution in methanol (15 mL). The white powder was immediately formed. After stirring the mixture for several hours, the solution was concentrated to dryness. The residue was washed with water and methanol (0.330 g, 56% yield). Anal. Calcd. for $C_{20}H_{30}CdS_2Cl_{0.5}Na_{0.5}$ (**6** · 0.5NaCl): C, 50.44; H, 6.35%. Found: C, 50.69; H, 6.41%. IR ν/cm^{-1} (KBr): 2908vs, 2846m, 1448w, 1295w, 1101w, 1036m, 827w, 682w. far-IR ν/cm^{-1} (CsI): 476m, 359vs, 280vs, 264m, 152s. Raman shift ν/cm^{-1}: 481w, 449s, 400w, 362m, 258vs. UV–Vis λ/nm (solid): 254.

4.2. Crystallography

Crystal data and refinement parameters for **4** are given in Table 3. The diffraction data were measured on a Rigaku/MSC Mercury CCD system with graphite monochromated Mo Kα ($\lambda = 0.71069$ Å) radiation at −61 °C. The crystal was mounted on glass fiber by epoxy glue. The unit cell parameters of the crystal were retrieved using Rigaku Daemon software and refined using CrystalClear on all observed reflections [56]. Data using 0.5° intervals in ϕ and ω for 20 s/frame were collected with a maximum resolution of 0.77 Å (744 oscillation images). The highly redundant data sets were reduced using CrystalClear and corrected for Lorentz and polarization effects. An empirical absorption correction was applied. Structures were solved by direct-methods using the program SIR 92 [57]. The position of the metal atoms and their first coordination sphere were located from the *E*-map; other non-hydrogen atoms were found in alternating difference Fourier syntheses (DIRDIF-99) [58] and least-squares refinement cycles and during the final cycles, were refined anisotropically (CrystalStructure) [59,60]. Hydrogen atoms were placed in calculated positions.

4.3. Measurements of zinc and sulfur K-edge EXAFS

The zinc and sulfur K-edge EXAFS data of **1**–**6** were recorded on bending magnet beam line 7C and 9A [61,62], respectively, at KEK Photon Factory, Tsukuba, Japan. Ring operation conditions were 2.5 GeV and 440–300 mA. Double Si(1 1 1) crystals were used as the monochromator. For the curve fit analyses, the empirical parameters of backscattering amplitudes and phase shifts for **5** and **6** were extracted from the EXAFS data for **2** and **3** (see below). Sample preparation was carried out under ambient condition. To avoid any artifacts of sample preparations, we checked the data reproducibility and tried to obtain the best spectra by more than three independent measurements for zinc K-edge and more than five independent measurements for sulfur K-edge. The zinc K-edge EXAFS data was collected in the transmission mode under ambient condition for finely powdered samples. The energy at the zinc K-edge was referred to the value for Zn foil at 9660 eV. The sulfur K-edge EXAFS data were collected by standard fluorescence detection techniques using a Lytle detector on finely powdered samples, which were spread thin and as uniform as possible [63]. The sample was kept under helium gas at room temperature during measurement. The first intense pre-edge peak for $Na_2S_2O_3 \cdot 5H_2O$ was referred to 2472.02 eV. The program of REX2000 [64] was used to extract the EXAFS signal and to analyze the data. Least-squares refinements of the structural parameters of the complexes were carried out against the k^3-weighted EXAFS signal to minimize the fit index. The cadmium K-edge is the borderline where this EXAFS experiment is possible at KEK Photon Factory. The cadmium K-edge measurements for complexes **3**, **4**, and **6** are in progress at SPring-8 but they are not reported in this paper.

Table 3
Crystallographic data of $(Et_4N)_2[\{Cd(ScHex)\}_4(\mu\text{-}ScHex)_6]$ (**4**)

Complex	**4** · 4.5MeCN
Formula	$C_{85}H_{163.50}Cd_4N_{6.50}S_{10}$
FW	2047.01
Crystal system	Monoclinic
Space group	$P2_1/n$ (No. 14)
a (Å)	14.879(6)
b (Å)	29.413(11)
c (Å)	24.720(9)
β (°)	110.988(4)
V (Å^3)	10,101.0(66)
Z	4
D_{calc} (g cm^{-3})	1.346
μ (Mo Kα) (cm^{-1})	10.80
Temperature (°C)	−61
2θ Range (°)	6–55
Reflections collected	81,032
Unique reflections	22,525
R_{int}	0.063
Number of observations	12,159 ($I > 2\sigma(I)$)
Number of variables	966
Final R, R_w[a]	0.060, 0.086
Maximum/minimum peak (e Å^{-3})	1.01/−0.78

[a] $R = \sum \|F_o| - |F_c\| / \sum |F_o|$; $R_w = [(\sum w(|F_o| - |F_c|)^2 / \sum wF_o^2)]^{1/2}$, $w = 1/\sigma^2(|F_o|)$.

4.4. Curve fit analyses of zinc and sulfur K-edge EXAFS

Empirical back scattering and phase shifts of parameters for the zinc K-edge EXAFS were extracted from **1** for Zn–S and Zn–C bonds, and from **2** for Zn···Zn interaction. Theoretical parameters were used based on McKale for Zn···C interactions [65]. Debye–Waller factors for model parameters were set to 0.06 Å. The crystallographic data for **1** and **2** were based on Ref. [11]. For **1**, the greatest peak in the range of 1.534–2.362 Å was defined to Zn–S of 2.262 Å. Another peak in the range of 2.976–3.528 Å was defined to Zn···C of 3.585 Å. For **2**, the peak in the range of 2.700–3.160 Å was defined to Zn···Zn of 3.312 Å and that in the range of 3.160–3.559 Å was defined to Zn···C of 3.625 Å. The fitting parameters in **5** were used based on the back scattering and phase shifts of **2** for Zn–S and Zn···Zn, and McKale for Zn···C [65].

The fit parameter for S–C, S–Zn, S–Cd, S···C_{far}, and S···S were extracted from the EXAFS data of complex **2** and **3** or theoretical parameters (McKale) [65]. The sulfur K-edge energy is relatively low (2471 eV) compared with that of metal, the obtained intensity is relatively low. Thus, we only discussed short-range S···S distances. Debye–Waller factors for model parameters were set to 0.06 Å. The corresponding bond distances of **2** and **3** are obtained from each crystal structure in the references [11,31]. For the complex **2**, the peak in the range of 0.920–1.902 Å was defined to S–C of 1.831 Å, and that in the range of 1.902–2.792 Å was defined to S–Zn of 2.352 Å. The peaks in the range of 2.792–3.375 Å and in the range of 3.375–3.958 Å were defined to S···C_{far} of 2.779 Å and S··· S of

3.864 Å, respectively. The shells used for **3** were S–C of 1.848 Å in the range of 0.951–1.963 Å, S–Cd of 2.550 Å in the range of 1.902–3.007 Å, S···C_{far} of 2.75 Å in the range of 3.007–3.958 Å, and S···S of 4.136 Å in the range of 3.958–4.449 Å. The distances of S···C_{far} and S···S were used by crystallographic data [14]. For the curve fitting of **5** in Fig. 9, the back scatterings and phase shifts of S–Zn, S–C and S···S of **2** are used as experimental parameters and McKale is used for S···C_{far} interaction as theoretical parameter. The curve fitting of **6** in Fig. 10 was performed by using the back scatterings and phase shifts of S–Cd and S–C of **3** as experimental parameters and of S···C_{far} and S···S interaction as McKale [65]. In these data fits, the threshold energy shifts were found to between 7.7 and −12.2 eV for the shells fit with empirical parameters. The shift values were between 9.1 and −14.5 eV for the shells fit with McKale parameters (Zn···C, S···C_{far}, and S···S). Thus, the fits using MaKale parameters were rationalized. Debye–Waller factors in **3** and **6** were very small. One possible reason for these strange factors is pinhole effects, which was sometimes observed in the same experimental conditions.

Acknowledgments

We thank Professor K. Tanaka of Institute of Molecular Science for FT-Raman measurements. This research was in part supported by Grant-in-Aid for Scientific Research (Nos. 11640555, 13555257, and 14540510) from Japan Society for the Promotion of Science, and the 21st Century COE (Center of Excellence) program (Promotion of Creative Interdisciplinary Materials Science for Novel Functions) from Ministry of Education, Culture, Sports, Science and Technology. Finally, we appreciate the kind editing of this manuscript by Dr. Peng Chen of Harvard University.

Appendix A. Supplementary data

Crystallographic data have been deposited at the CCDC, 12 Union Road, Cambridge CB2 1EZ, UK and copies can be obtained on request, free of charge, by quoting the publication citation and the deposition numbers 260804. Supplementary data associated with this article (zinc K-edge EXAFS data with each fitting data (Figs. S1–S3) and the obtained radial distances, Debye–Waller factors and coordination numbers (Table S1)) can be found, in the online version at doi:10.1016/j.jinorgbio.2005.11.004.

References

[1] G. Henkel, B. Krebs, Chem. Rev. 104 (2004) 801–824.
[2] I.G. Dance, Polyhedron 5 (1986) 1037–1104.
[3] P.J. Blower, J.R. Dilworth, Coord. Chem. Rev. 76 (1987) 121–185.
[4] Y. Zhang, S. Mukherjee, E. Oldfield, J. Am. Chem. Soc. 127 (2005) 2370–2371.
[5] S. Lipton, C. Bergquist, G. Parkin, P.D. Ellis, J. Am. Chem. Soc. 125 (2003) 3768–3772.
[6] M.F. Summers, Coord. Chem. Rev. 86 (1988) 43–134.
[7] L.M. Utschig, J.W. Bryson, T.V. O'Halloran, Science 268 (1995) 380–385.
[8] G. Fleissner, P.M. Kozlowski, M. Vargek, J.W. Bryson, T.V. O'Halloran, T.G. Spiro, Inorg. Chem. 38 (1999) 3523–3528.
[9] Y. Matsunaga, K. Fujisawa, N. Amir, Y. Miyashita, K. Okamoto, J. Coord. Chem. 58 (2005) 1047–1061.
[10] Y. Matsunaga, K. Fujisawa, N. Amir, Y. Miyashita, K. Okamoto, Appl. Organomet. Chem. 19 (2005) 778–789.
[11] Y. Matsunaga, K. Fujisawa, N. Ibi, N. Amir, Y. Miyashita, K. Okamoto, Bull. Chem. Soc. Jpn. 78 (2005) 1285–1287.
[12] E.I. Solomon, B. Hedman, K.O. Hodgson, A. Dey, R.K. Szilagyi, Coord. Chem. Rev. 249 (2005) 97–129.
[13] T. Glaser, B. Hedman, K.O. Hodgson, E.I. Solomon, Acc. Chem. Res. 33 (2000) 859–868.
[14] J.E. Penner-Hahn, Coord. Chem. Rev. 249 (2005) 161–177.
[15] A. Vogel, O. Schilling, W. Meyer-Klaucke, Biochemistry 43 (2004) 10379–10386.
[16] D.A. Tobin, J.S. Pickett, H.L. Hartman, C.A. Fierke, J.E. Penner-Hahn, J. Am. Chem. Soc. 125 (2003) 9962–9969.
[17] S. Priggemeyer, P. Eggers-Borkenstein, F. Ahlers, G. Henkel, M. Körner, H. Witzel, H.-F. Nolting, C. Hermes, B. Krebs, Inorg. Chem. 34 (1995) 1445–1454.
[18] J.L. Thorvaldsen, A.K. Sewell, A.M. Tanner, J.M. Peltier, I.J. Pickering, G.N. George, D.R. Winge, Biochemistry 33 (1994) 9566–9577.
[19] R.A.D. Pattrick, J.F.W. Mosselmans, J.M. Charnock, Eur. J. Mineral. 10 (1998) 239–249.
[20] H. Hosokawa, K. Murakoshi, Y. Wada, S. Yanagida, M. Satoh, Langmuir 12 (1996) 3598–3603.
[21] Q. Zhou, T.W. Hambley, B.J. Kennedy, P.A. Lay, Inorg. Chem. 42 (2003) 8557–8566.
[22] J.-S. Kim, M. Ree, T.J. Shin, O.H. Han, S.J. Cho, Y.-T. Hwang, J.Y. Bae, J.M. Lee, R. Ryoo, H. Kim, J. Catal. 218 (2003) 209–219.
[23] J.M. Corker, J. Evans, J. Chem. Soc., Chem. Commun. (1994) 1027–1029.
[24] C.E. Hayter, J. Evans, J.M. Corker, R.J. Oldman, B.P. Williams, J. Mater. Chem. 12 (2002) 3172–3177.
[25] S.J. Hibble, R.I. Walton, M.R. Feaviour, A.D. Smith, J. Chem. Soc., Dalton Trans. (1999) 2877–2883.
[26] P. Roubin, S. Varin, C. Crépin, B. Gauthier-Roy, A.-M. Flank, R. Delaunay, M. Pompa, B. Tremblay, J. Chem. Phys. 109 (1998) 7945–7948.
[27] J. Evans, J.M. Corker, C.E. Hayter, R.J. Oldman, B.P. Williams, Chem. Commun. (1996) 1431–1432.
[28] S.J. Hibble, R.I. Walton, D.M. Pickup, J. Chem. Soc., Dalton Trans. (1996) 2245–2251.
[29] S. Maeyama, M. Sugiyama, S. Huen, M. Oshima, J. Cryst. Growth 150 (1995) 1122–1125.
[30] Z. Gui, A.R. Green, M. Kasrai, G.M. Bancroft, M.J. Stillman, Inorg. Chem. 35 (1996) 6520–6529.
[31] J. Sola, P. Gonzáles-Duarte, J. Sanz, I. Casals, T. Alsina, I. Sobrados, A. Alvarez-Larena, J.-F. Piniella, X. Solans, J. Am. Chem. Soc. 115 (1993) 10018–10028.
[32] T. Costa, J.R. Dorfman, K.S. Hagen, R.H. Holm, Inorg. Chem. 22 (1983) 4091–4099.
[33] K.S. Hagen, J.G. Reynolds, R.H. Holm, J. Am. Chem. Soc. 103 (1981) 4045–4063.
[34] K.S. Hagen, J.M. Berg, R.H. Holm, Inorg. Chim. Acta 45 (1980) L17–L18.
[35] I.G. Dance, J. Am. Chem. Soc. 101 (1979) 6264–6273.
[36] I.G. Dance, J.C. Calabrese, J. Chem. Soc., Chem. Commun. (1975) 762–763.
[37] Z.-X. Huang, H.-Y. Hu, W.-Q. Gu, G. Wu, J. Inorg. Biochem. 54 (1994) 147–155.
[38] J.L. Hencher, M.A. Khan, F.F. Said, D.G. Tuck, Polyhedron 4 (1985) 1263–1267.
[39] K.S. Hagen, R.H. Holm, Inorg. Chem. 22 (1983) 3171–3174.

[40] S.L. Guo, E. Ding, S.M. Liu, Y.Q. Yin, J. Inorg. Biochem. 70 (1998) 7–10.
[41] P.A.W. Dean, J.J. Vittal, Inorg. Chem. 26 (1987) 278–283.
[42] I.G. Dance, A. Choy, M.L. Scudder, J. Am. Chem. Soc. 106 (1984) 6285–6295.
[43] A. Choy, D. Craig, I. Dance, M. Scudder, J. Chem. Soc., Chem. Commun. (1982) 1246–1247.
[44] P.A.W. Dean, N.C. Payne, J. Wranich, J.J. Vittal, Polyhedron 17 (1998) 2411–2416.
[45] I.G. Dance, Inorg. Chem. 20 (1981) 2155–2160.
[46] P.A.W. Dean, J.J. Vittal, Y. Wu, Can. J. Chem. 70 (1992) 779–791.
[47] P.A.W. Dean, J.J. Vittal, N.C. Payne, Inorg. Chem. 26 (1987) 1683–1689.
[48] P.A.W. Dean, N.C. Payne, J.J. Vittal, Y. Wu, Inorg. Chem. 32 (1993) 4632–4639.
[49] I.G. Dance, J. Am. Chem. Soc. 102 (1980) 3445–3451.
[50] T. Løver, G.A. Bowmaker, J.M. Seakins, R.P. Cooney, Chem. Mater. 9 (1997) 967–975.
[51] I.L. Abraham, C.D. Garner, W. Clegg, J. Chem. Soc., Dalton Trans. (1987) 1577–1579.
[52] A.D. Watson, C.P. Rao, J.R. Dorfman, R.H. Holm, Inorg. Chem. 24 (1985) 2820–2826.
[53] W.L.F. Armarego, D.D. Perrin, Purification of Laboratory Chemicals, fourth ed., Butterworth-Heinemann, Oxford, 1997.
[54] K.K. Khullar, L. Bauer, J. Org. Chem. 36 (1971) 3038–3040.
[55] J.M. Kokosa, L. Bauer, R.S. Egan, J. Org. Chem. 40 (1975) 3196–3199.
[56] CrystalClear Ver. 1.3., J.W. Pflugrath, Acta Crystallogr. D55 (1999) 1718.
[57] A. Altomare, G. Cascarano, C. Giacovazzo, A. Guagliardi, M. Burla, G. Polidori, M. Camalli, J. Appl. Crystallogr. 27 (1994) 435.
[58] P.T. Beurskens, G. Admiraal, G. Beurskens, W.P. Bosman, R. de Gelder, R. Israel, J.M.M. Smits, The DIRDIF-99 program system, Technical Report of the Crystallography Laboratory, University of Nijmegen, The Netherlands, 1999.
[59] CrystalStructure 3.51: Crystal Structure Analysis Package, Rigaku and Rigaku/MSC, 2003.
[60] Crystal Issue 10: D.J. Watkin, C.K. Prout, J.R. Carruthers, P.W. Betteridge, Chemical Crystallography Laboratory, Oxford, UK, 1996.
[61] M. Nomura, A. Koyama, M. Sakurai, KEK Report 91 (1) (1991) 1–21.
[62] M. Nomura, A. Koyama, J. Synchrotron Rad. 6 (1999) 182–184.
[63] Y. Izumi, T. Minato, K. Aika, A. Ishiguro, T. Nakajima, Y. Wakatsuki, Studies in Surface Science and Catalysis, in: E. Gaigneaux, D.E. De Vos, P. Grange, P.A. Jacobs, J.A. Martens, P. Ruiz, G. Poncelet (Eds.), Scientific Bases for the Preparation of Heterogeneous Catalysts, vol. 143, Elsevier, Amsterdam, 2002, pp. 361–368.
[64] XAFS analysis software ver. 2.04: REX2000 for Windows, Rigaku (2000).
[65] A.G. McKale, B.W. Veal, A.P. Paulikas, S.-K. Chan, G.S. Knapp, J. Am. Chem. Soc. 110 (1988) 3763–3768.